ORIGINAL PAPER

V.N. Tikhonovich · E.N. Naumovich · D.I. Logvinovich
V.V. Kharton · A.A. Vecher

Oxygen deficiency and phase transitions in $SrCo_{1-x-y}Fe_xCr_yO_{3-\delta}$ (x = 0.10–0.40, y = 0–0.05)

Abstract Oxygen-deficient phases based on perovskite-like strontium cobaltites-ferrites are promising mixed conductors for high-temperature electrochemical applications. The $p(O_2)$-T-δ diagrams for the oxide systems $SrCo_{1-x-y}Fe_xCr_yO_{3-\delta}$ (x = 0.10–0.40; y = 0–0.05) were studied at 500–1000 °C in the oxygen pressure range from 10^{-5} to 0.21 atm using the coulometric titration technique and thermogravimetric analysis. Stability limits of the cubic perovskite phases having a high oxygen ionic conductivity were evaluated as functions of temperature, oxygen partial pressure and oxygen non-stoichiometry. It was found that doping with chromium and increasing the iron content in $SrCo(Fe,Cr)O_{3-\delta}$ both lead to a considerable enlargement of the cubic perovskite phase existence domain towards lower temperatures and reduced oxygen pressures.

Introduction

Oxygen-deficient perovskite-like solid solutions, based on strontium cobaltite, possess very high oxygen ion mobility combined with predominantly electronic conduction and are thus of interest for applications in mixed-conducting ceramic membranes for high-purity oxygen separation [1, 2, 3, 4]. Under the operating

---

V.N. Tikhonovich (✉) · E.N. Naumovich · D.I. Logvinovich · V.V. Kharton · A.A. Vecher
Institute for Physical Chemical Problems, Belarus State University, 14 Leningradskaya Str., 220050 Minsk, Belarus
E-mail: vtikhonovich@by.kyriba.com

Present address: V.V. Kharton
Department of Ceramics and Glass Engineering, UIMC, University of Aveiro, 3810-193 Aveiro, Portugal

conditions, ceramic membranes are exposed to different atmospheres and subjected to severe mechanical and thermal stresses. The oxygen nonstoichiometry and phase transitions, which may be induced by the nonstoichiometry variations, play a vital role in the membrane stability [5]. Therefore, the development of ceramic membrane materials requires systematic studies of their oxygen deficiency as a function of the oxygen partial pressure and temperature, in conjunction with other stability tests.

The objective of the present study was to study oxygen nonstoichiometry in the oxide systems $SrCo_{1-x-y}Fe_xCr_yO_{3-\delta}$ (x = 0.10, 0.20, 0.40; y = 0, 0.01, 0.03, 0.05) and to evaluate the stability limits of the perovskite-type phases having a high oxygen permeability [3, 4, 6, 7].

Experimental

Sample preparation

All studied materials were prepared by a standard ceramic synthesis route using $CoSO_4 \cdot 7H_2O$, $FeC_2O_4 \cdot 2H_2O$, $(NH_4)_2Cr_2O_7$ and $SrCO_3$ as precursors. Cobalt sulfate was preliminary decomposed in order to prevent $SrSO_4$ formation. The solid state reactions were performed in air at 950–1150 °C with several intermediate grinding steps. The synthesized compositions and their abbreviations are listed in Table 1.

Ceramic samples in the shape of bars (4×4×20 mm³) and pellets (thickness of 2–4 mm, diameter 15 mm) were pressed (300–600 MPa) and then sintered in air at 1200–1300 °C over 10–30 h. The phase composition and structure of the sintered samples were determined by X-ray diffraction analysis (Cu K_α radiation, $\bar{\lambda}_\alpha$ = 1.54178 nm). After synthesis in air, the compositions $SrCo_{0.8}Fe_{0.2}O_{3-\delta}$, $SrCo_{0.6}Fe_{0.4}O_{3-\delta}$, $SrCo_{0.87}Fe_{0.10}Cr_{0.03}O_{3-\delta}$ and $SrCo_{0.85}Fe_{0.10}Cr_{0.05}O_{3-\delta}$ were each a single phase with a cubic perovskite-type structure. Detailed information on the phase composition and structure of all the prepared materials can be found in our previous papers [7, 8, 9].

Thermogravimetry

Thermogravimetric measurements were carried out using a high-temperature device based on an analytical balance, VLA-200g-M (accuracy limit 0.1 mg). Pre-calcified quartz sample holders

Table 1 Abbreviations used for $SrCo_{1-x-y}Fe_xCr_yO_{3-\delta}$ compositions

y	x	Abbreviation
0	0.10	Cr0
0.01	0.10	Cr1
0.03	0.10	Cr3
0.05	0.10	Cr5
0	0.20	CoFe20
0	0.40	CoFe40

(hemispheres suspended on balances on a quartz string) were preliminary calibrated against routine influences on apparent weight under the conditions close to the planned experiment, including the temperatures, gas flux and composition of the gas mixtures.

The total oxygen content was determined by reduction in a dry hydrogen flow at 950–1000 °C. The oxygen content [O] in a sample under study was calculated as:

$$[O] = [O]_{red} + \frac{m_0 - m_{red}}{15.9994} \Big/ \frac{m_{red}}{M_{red}} \tag{1}$$

where m_0 is the starting weight of the sample, m_{red} is the sample weight after reduction, M_{red} is the molar mass of the reduced form of a given material, and $[O]_{red}$ is the oxygen content in the reduced form. $[O]_{red}$ was calculated by presuming that, after reduction, cobalt and iron are in metallic form, and the oxidation state of Cr and Sr cations is $3+$ and $2+$, respectively, in agreement with thermodynamic data. The reduced form of $SrCo_xFe_yCr_zO_{3-\delta}$ can therefore be written as $SrCo_xFe_yCr_zO_{1+1.5z}$.

Coulometric titration

The coulometric titration of oxygen was carried out in two-electrode cells made of $Zr_{0.90}Y_{0.10}O_{1.95}$ (YSZ) solid electrolyte. Platinum electrodes, marked as 3 in Fig. 1, were alternately used for oxygen pumping and for determination of the oxygen partial pressure inside the cell. The samples placed in the lower zirconia cap were weighed immediately prior to the cell installation (Fig. 1). After installation, the cells were sealed at 1200 °C and then slowly cooled to the working temperatures (upper limit of about 900 °C).

The oxygen partial pressure inside the measuring cells, p, was calculated by the Nernst equation:

$$p = p_0 \exp\left[-\frac{4FE}{RT}\right] \tag{2}$$

where p_0 is the oxygen partial pressure at the air reference electrode, and E is the e.m.f. between the cell electrodes, measured after overpotential relaxation.

The total oxygen content in the cells was varied by passing a direct electrical current between the electrodes (galvanostatic mode). Typical values of the current (I) varied in range 250–500 µA, with an accuracy of 0.5 µA. The amount of pumped oxygen, γ_{O_2}, was calculated by Faraday's law:

$$\gamma_{O_2} = \frac{I\tau}{4F} \tag{3}$$

where τ is the duration of the galvanostatic step. The overpotential relaxation time after pumping was, as a rule, about 1.5 h. Oxygen nonstoichiometry changes after a galvanostatic step were calculated as:

$$\delta_2 = \delta_1 \pm 2\gamma_{O_2}\frac{M_0}{m_0} \tag{4}$$

where δ_1 and δ_2 are the oxygen deficiency before and after pumping, respectively, γ_{O_2} is the amount of pumped oxygen, M_0 is the molar mass of the oxide at room temperature, and m_0 is the sample weight at room temperature, determined prior to sealing.

After oxygen pumping and subsequent equilibration, the cell e.m.f. was measured as a function of temperature (steps of 20–35 °C). In the course of the temperature variations, the change of the oxygen content in a sample is equal to that in the gas phase inside the cell, calculated as:

$$n(T) = n(T_0) - \frac{V}{R}\left(\frac{p}{T} - \frac{p_0}{T_0}\right) \tag{5}$$

where $n(T)$ and $n(T_0)$ correspond to the amount of gaseous oxygen in the cell at temperatures T and T_0, respectively, p and p_0 are the oxygen partial pressures at these temperatures, and V is the free volume of the cell, measured before each experiment.

Oxygen leakage determination

Oxygen leakage into a measuring cell is the main source of errors in the coulometric titration experiments. The leakage may result either from the so-called electrolytic permeation due to the minor electronic conductivity of zirconia under high oxygen chemical potential gradients, or from gas flows through microcracks in the solid-electrolyte ceramics and sealing. One possible solution of this problem is to decrease the size of the cell and especially its open surface. In the present work, cells with an internal volume of about 0.15 cm^3 were used. Figure 2 presents an example of the relaxation processes in one empty measuring cell. Notice that such a long
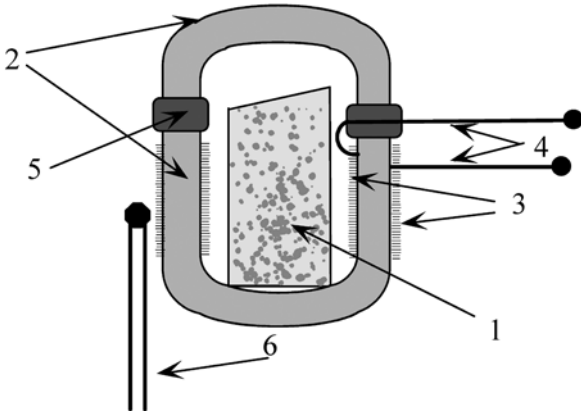

Fig. 1 Schematic drawing of the electrochemical cell for coulometric titration: *1*, porous ceramic sample; *2*, solid-electrolyte caps; *3*, Pt electrodes; *4*, Pt wires; *5*, glass-ceramic sealant; *6*, thermocouple
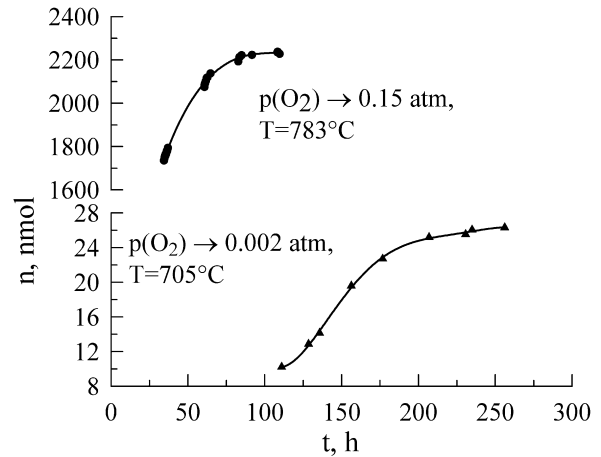

Fig. 2 Examples of oxygen leakage into an empty cell for coulometric titration

transient time is typical only for empty cells, probably due to a significant adsorptive capacity of highly porous Pt electrodes with respect to the cell volume [10]. For the cells with samples inside, the transient times after a temperature variation step did not exceed 20–30 min. The calculated oxygen leakage fluxes were about 10^{-15}–10^{-14} mol/s (i.e. lower than 10 nA).

Results and discussion

Thermal analysis

Temperature dependences of the total oxygen content in $SrCo(Fe,Cr)O_{3-\delta}$ in air, determined by thermal gravimetric analysis (TGA), are presented in Figs. 3 and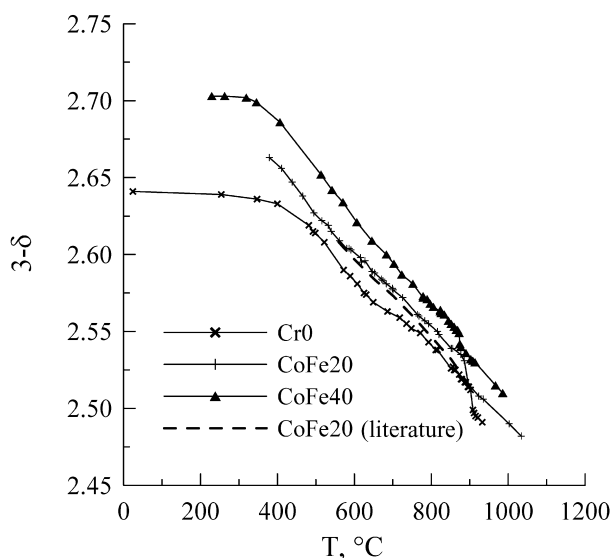 4. The values of the oxygen nonstoichiometry of $SrCo_{0.8}Fe_{0.2}O_{3-\delta}$ obtained in this work are in good agreement with literature data [11]. As expected, incorporation of iron cations in the perovskite lattice results in a greater average oxidation state of the B-site cations with respect to undoped strontium cobaltite, increasing as $SrCo_{0.9}Fe_{0.1}O_{3-\delta} < SrCo_{0.8}Fe_{0.2}O_{3-\delta} < SrCo_{0.6}Fe_{0.4}O_{3-\delta}$ (Fig. 3). A similar effect is observed when cobalt is substituted by chromium (Fig. 4), which results, in particular, from the high stability of octahedrally coordinated Cr^{4+} cations in the perovskite lattice [12].

TGA showed that all studied materials are characterized with a drastic decrease of the oxygen content at 890 ± 10 °C, when the variation in δ values is as high as 0.02. At similar temperatures, differential thermal analysis (DTA) shows an explicit endothermic effect; the data on $SrCo_{0.9}Fe_{0.1}O_{3-\delta}$ as an example are presented in Fig. 5. Such behavior may be attributed to phase changes induced by oxide reduction on heating, as discussed below. One should also mention a plateau, observed on the TGA curve of $SrCo_{0.9}Fe_{0.1}O_{3-\delta}$ at 600–700 °C, and the corresponding small endothermic peak in DTA curves. The latter phenomenon was found only for $SrCo_{0.9}Fe_{0.1}O_{3-\delta}$ and was ascribed to the phase instability of this composition at low temperatures, confirmed by the coulometric titration and XRD data.

Phase stability boundaries

One example of the temperature dependence of the equilibrium oxygen partial pressure over $SrCo_{0.9}Fe_{0.1}O_{3-\delta}$, typical for $SrCoO_{3-\delta}$-based solid solutions, is presented in Fig. 6; the indexes on the curves denote the total oxygen content. The $p(O_2)$-T-δ diagram consists of

Fig. 3 Temperature dependence of the total oxygen content in $Sr(Co,Fe)O_{3-\delta}$ in air. Literature data on $SrCo_{0.8}Fe_{0.2}O_{3-\delta}$ [11] are shown for comparison

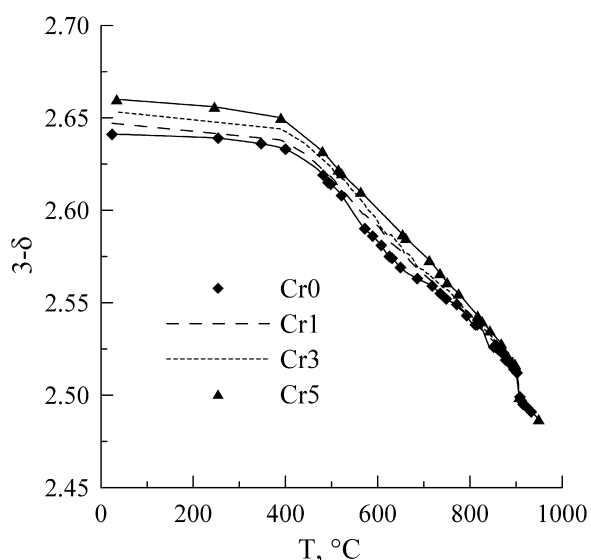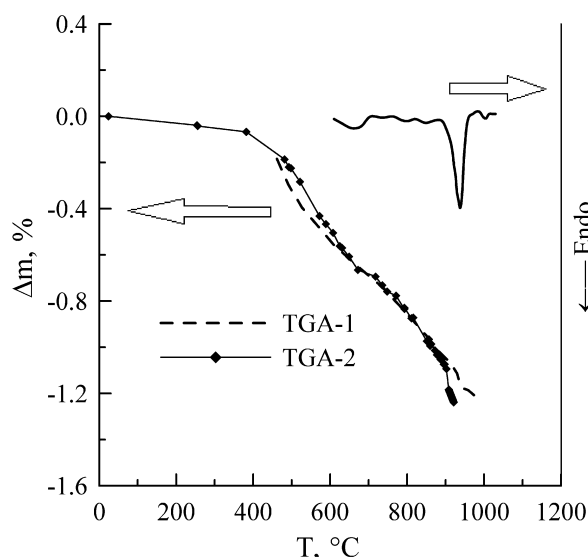**Fig. 4** The total oxygen content in $SrCo(Fe,Cr)O_{3-\delta}$ phases in air

Fig. 5 DTA and TGA curves (heating rate of 15 K/min) for $SrCo_{0.9}Fe_{0.1}O_{3-\delta}$ in air. The TGA-1 curve was obtained using DTA and TGA-2 represents the TGA results. The difference in the TGA curves at low temperatures is probably due to the formation of strontium carbonate on the surface of the samples
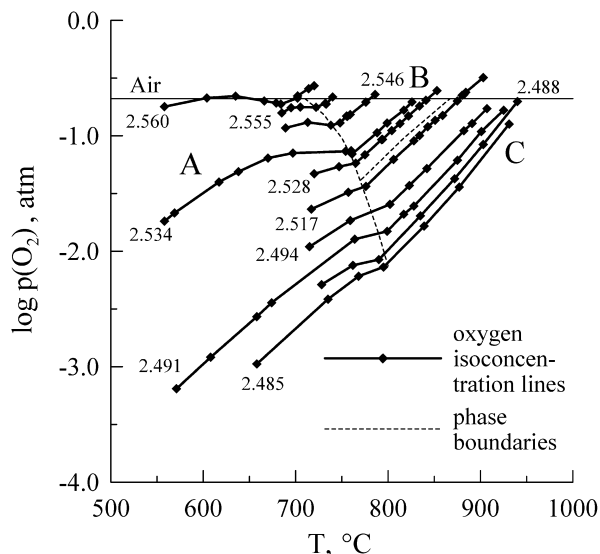
Fig. 6 The $p(O_2)$-T-δ diagram for $SrCo_{0.9}Fe_{0.1}O_{3-\delta}$. *Solid and dashed lines* correspond to the oxygen isoconcentration lines and phase boundaries, respectively

Fig. 7 Approximate phase boundaries estimated from the coulometric titration data. Domain *A* is below the phase stability limits marked by *solid lines*. Domains *B* and *C* are above these boundaries and correspond to the left and right sectors separated by *dashed line*, respectively

three domains, marked as A, B and C. When the oxygen content is close to a boundary between these domains, a drastic nonstoichiometry variation, extremely slow equilibration [11] and hysteresis phenomena are observed. As found by XRD, the B domain relates to the cubic perovskite solid solution. The boundary between the B and C domains is close to the oxygen isoconcentration line with $3-\delta \approx 2.519$, in agreement with literature data [11]. A similar location of the B-C boundary is characteristic of $SrCo_{0.80}Fe_{0.20}O_{3-\delta}$ and $SrCo_{0.90-y}Fe_{0.10}Cr_yO_{3-\delta}$ with $y = 0$–0.03 (Fig. 7).

Figure 7 shows approximate phase stability limits estimated from the coulometric titration data. For $SrCo_{0.9}Fe_{0.1}O_{3-\delta}$, the line between the A and B domains reaches atmospheric oxygen pressure at temperatures close to 700 °C. This is reflected as the plateau and endothermic effect on TGA and DTA curves, respectively (Fig. 5), and corresponds to decomposition of the cubic perovskite phase on cooling in air, found by XRD. Increasing either the chromium or iron concentration in the $SrCo(Fe,Cr)O_{3-\delta}$ lattice leads to an enlargement of the cubic perovskite phase existence domain (B) towards lower temperatures and reduced $p(O_2)$. The cubic phases of $SrCo_{0.80}Fe_{0.20}O_{3-\delta}$ and $SrCo_{0.87}Fe_{0.10}Cr_{0.03}O_{3-\delta}$ are sufficiently stable in air: their A-B boundaries in the studied temperature range lie at lower oxygen partial pressures. However, the A-B phase boundary of $SrCo_{0.80}Fe_{0.20}O_{3-\delta}$ might approach atmospheric oxygen pressure at approximately 550 °C. This temperature is critical for oxygen exchange between the oxide and gas phase; at lower temperatures, phase transitions induced by the oxygen nonstoichiometry variations may be frozen. Therefore, at room temperature the cubic perovskite phase of $SrCo_{0.80}Fe_{0.20}O_{3-\delta}$ could be metastable.

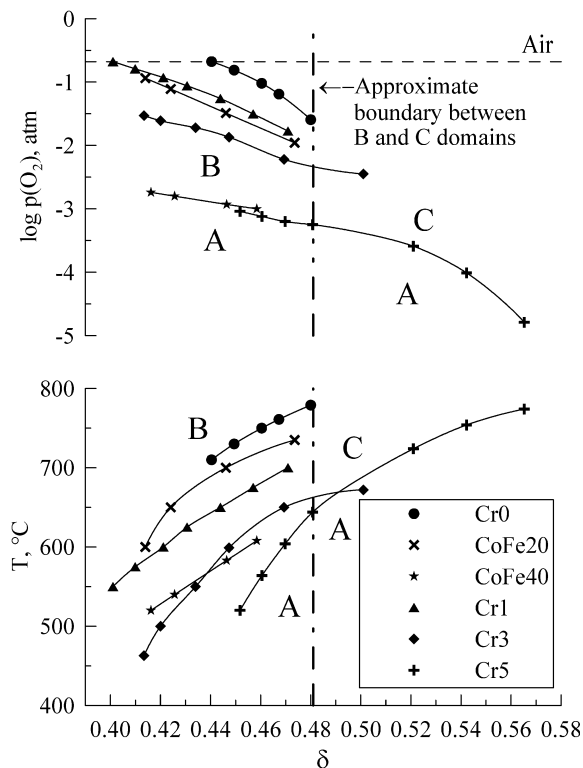The data on oxygen deficiency (Figs. 8 and 9) show that, for all studied phases, transition between the B and

C domains starts at definite critical values of the oxygen vacancy concentration, which are essentially independent of temperature. In the case of Cr-containing materials, these critical values of δ are close to 0.481 (Fig. 7).

Phase composition and structure

When discussing phase changes corresponding to the B-C boundary (Fig. 3), one should note that the literature information on the crystal structure of $SrCoO_{3-\delta}$-based materials at temperatures above 900 °C is very limited. For instance, the structure of strontium cobaltite has been reported as brownmillerite [11] and as distorted perovskite [13]. Structure refinement of $SrCoO_{3-\delta}$-based compounds is often complicated owing to disorder in the cation sublattices of oxygen-deficient phases, their structural similarity and insufficient sensitivity of XRD with respect to the oxygen sublattice. Neutron diffraction studies [14] showed that strontium cobaltite, having a brownmillerite-type lattice at temperatures above 900 °C, forms a hexagonal $Sr_6Co_5O_{15}$ phase on cooling.

In this work, similar behavior was observed for the $SrCo_{0.85}Fe_{0.10}Cr_{0.05}O_{3-\delta}$ composition, studied as a model phase. Figure 10 presents several representative examples of XRD patterns for $SrCo_{0.85}Fe_{0.10}Cr_{0.05}O_{3-\delta}$,
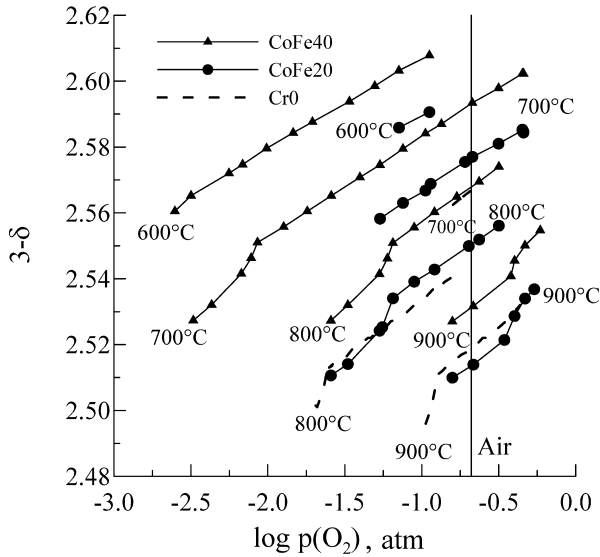
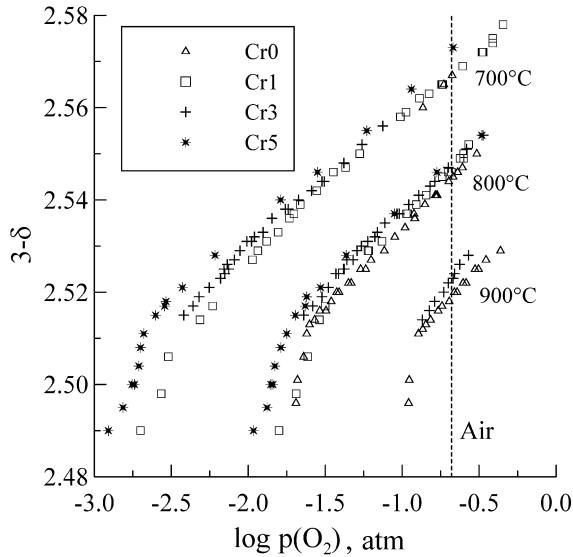**Fig. 8** Total oxygen content in $SrCo(Fe)O_{3-\delta}$ as a function of the oxygen partial pressure

Fig. 9 Oxygen partial pressure dependence of the total oxygen content in $SrCo(Fe,Cr)O_{3-\delta}$

Fig. 10 XRD patterns of $SrCo_{0.85}Fe_{0.10}Cr_{0.05}O_{3-\delta}$ powder annealed for 100 h at 840 °C in flowing O_2-Ar mixtures with different $p(O_2)$. The values of the oxygen partial pressure are given on the patterns

annealed for 100 h in atmospheres with various oxygen partial pressures at 840 °C. In the case of atmospheric air (Fig. 10A), the sample was cooled at a rate of 1.0–1.5 °C/min in order to obtain an equilibrium oxygen content. The samples annealed at other oxygen pressures were quenched. At 840 °C, the cubic phase of $SrCo_{0.85}Fe_{0.10}Cr_{0.05}O_{3-\delta}$ decomposes when $p(O_2)$ is lower than 0.04 atm (Fig. 10C and D). The decomposition products can be identified as a hexagonal strontium cobaltite-based phase (the strongest reflections are marked as 1 and 2 in Fig. 10D) and cobalt oxides CoO and Co_3O_4 (peaks 3 and 4, respectively). Taking into account the literature data [6] indicating that the hexagonal form of strontium cobaltite is stable at temperatures below
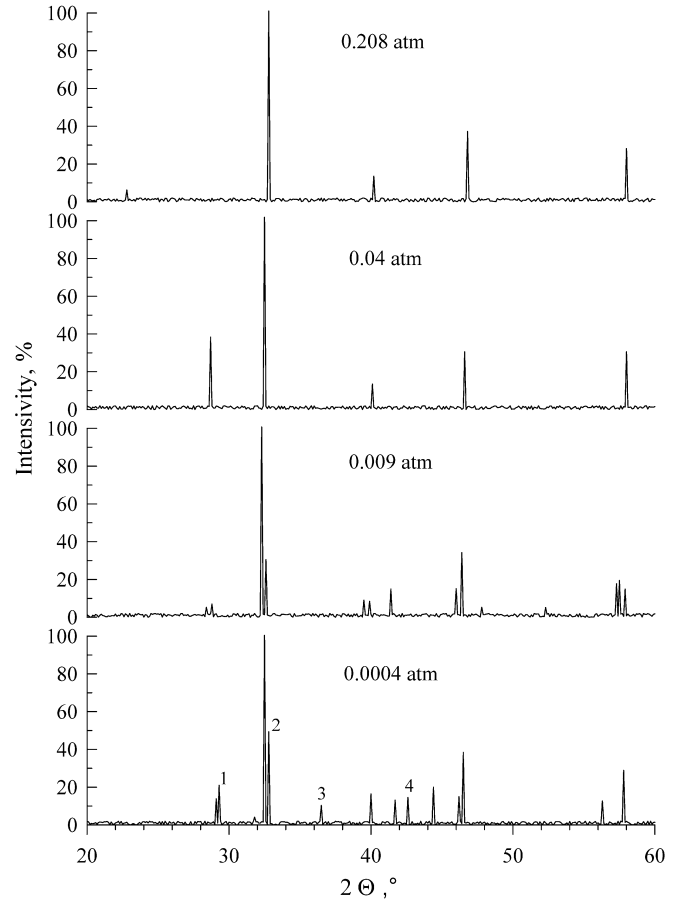
800 °C, one can assume that this phase is formed during the sample cooling.

For $SrCo_{0.80}Fe_{0.20}O_{3-\delta}$, a single cubic perovskite phase and a mixture of the brownmillerite-type and perovskite phases exist in the domains B and A, respectively [11]. Comparing the literature data with the approximate phase boundaries estimated from the coulometric titration results (Fig. 7), one can conclude that the A domain in the $p(O_2)$-T-δ diagrams of $SrCo(Fe,Cr)O_{3-\delta}$ corresponds to the products of cubic perovskite decomposition (a mixture of the perovskite and brownmillerite-type or hexagonal $Sr_6Co_5O_{15}$-based phases). Detailed studies of phase changes, which occur when the oxygen pressure is close to the B-C boundary, are now in progress.

Conclusions

The oxygen nonstoichiometry of chromium-substituted strontium cobaltites-ferrites, $SrCo_{1-x-y}Fe_xCr_yO_{3-\delta}$, was studied at 500–1000 °C and $p(O_2)=10^{-5}$ to 0.21 atm using coulometric titration and TGA methods. The

cubic perovskite-type phases, having high ionic conductivity and oxygen permeability, exist in a relatively narrow domain where the nonstoichiometry is lower than approximately 0.48. Substitution of cobalt by iron and chromium enlarges the stability domain of the perovskites towards lower temperatures and oxygen pressures. The perovskite phases $SrCo_{0.80}Fe_{0.20}O_{3-\delta}$ and $SrCo_{0.87}Fe_{0.1}Cr_{0.03}O_{3-\delta}$ are thermodynamically stable in air above 550 °C, but may be metastable at lower temperatures.

References

1. Bouwmeester HJM, Burgraaf AJ (1996) In: Burgraaf AJ, Cot L (eds) Fundamentals of inorganic membrane science and technology. Elsevier, Amsterdam, pp 435–528
2. Carter S, Selcuk A, Chater RJ, Kajda J, Kilner JA, Steele BCH (1992) Solid State Ionics 53–56:597
3. Kharton VV, Naumovich EN, Nikolaev AV (1996) J Membr Sci 111:149
4. Kharton VV, Yaremchenko AA, Kovalevsky AV, Viskup AP, Naumovich EN, Kerko PF (1999) J Membr Sci 163:307–317
5. Pei S, Kleefish MS, Kobylinski TP, Faber J, Udovich CA, Zhang-McCoy V, Dabrowski B, Balachandran U, Mieville RL, Poeppel RB (1995) Catal Lett 30:201–212
6. Qiu L, Lee TH, Liu LM, Yang YL, Jacobson AJ (1995) Solid State Ionics 76:321
7. Kharton VV, Tikhonovich VN, Li Shuangbao, Naumovich EN, Kovalevsky AV, Viskup AP, Bashmakov IA, Yaremchenko AA (1998) J Electrochem Soc 145:1363
8. Kharton VV, Zhuk PP, Demin AK, Nikolaev AV, Tonoyan AA, Vecher AA (1992) Inorg Mater 28:1406
9. Kharton VV, Naumovich EN, Nikolaev AV, Astashko VV, Vecher AA (1993) Russ J Electrochem 29:1039
10. Kuzin BL, Komarov MA (1991) In: Perfilyev MV (ed) Electrode processes of solid-state systems (in Russian). Academy of Sciences of USSR, Ural Dept., Sverdlovsk, pp 3–17
11. Liu LM, Lee TH, Qui L, Yang YL, Jacobson AJ (1996) Mater Res Bull 3:29
12. Mizusaki J (1992) Solid State Ionics 52:79
13. Vashook VV, Zinkevich MV, Zonov YuG (1999) Solid State Ionics 116:129
14. Harrison WTA, Hegwood SL, Jacobson AJ (1995) J Chem Soc Chem Commun 1953